Variations in northern vegetation activity inferred from satellite data of vegetation index during 1981 to 1999

Liming Zhou,[1] Compton J. Tucker,[2] Robert K. Kaufmann,[1] Daniel Slayback,[3] Nikolay V. Shabanov,[1] and Ranga B. Myneni[1]

Abstract. The northern high latitudes have warmed by about 0.8°C since the early 1970s, but not all areas have warmed uniformly [*Hansen et al.*, 1999]. There is warming in most of Eurasia, but the warming rate in the United States is smaller than in most of the world, and a slight cooling is observed in the eastern United States over the past 50 years. These changes beg the question, can we detect the biotic response to temperature changes? Here we present results from analyses of a recently developed satellite-sensed normalized difference vegetation index (NDVI) data set for the period July 1981 to December 1999: (1) About 61% of the total vegetated area between 40°N and 70°N in Eurasia shows a persistent increase in growing season NDVI over a broad contiguous swath of land from central Europe through Siberia to the Aldan plateau, where almost 58% (7.3×10^6 km^2) is forests and woodlands; North America, in comparison, shows a fragmented pattern of change in smaller areas notable only in the forests of the southeast and grasslands of the upper Midwest, (2) A larger increase in growing season NDVI magnitude (12% versus 8%) and a longer active growing season (18 versus 12 days) brought about by an early spring and delayed autumn are observed in Eurasia relative to North America, (3) NDVI decreases are observed in parts of Alaska, boreal Canada, and northeastern Asia, possibly due to temperature-induced drought as these regions experienced pronounced warming without a concurrent increase in rainfall [*Barber et al.*, 2000]. We argue that these changes in NDVI reflect changes in biological activity. Statistical analyses indicate that there is a statistically meaningful relation between changes in NDVI and land surface temperature for vegetated areas between 40°N and 70°N. That is, the temporal changes and continental differences in NDVI are consistent with ground-based measurements of temperature, an important determinant of biological activity. Together, these results suggest a photosynthetically vigorous Eurasia relative to North America during the past 2 decades, possibly driven by temperature and precipitation patterns. Our results are in broad agreement with a recent comparative analysis of 1980s and 1990s boreal and temperate forest inventory data [*United Nations*, 2000].

1. Introduction

Analysis of surface temperature recorded at meteorological stations shows that the global surface temperature in 1998 is the warmest and the rate of temperature change during the past 25 years is higher than in any previous period of the instrumental record [*Hansen et al.*, 1999], and possibly the past 6 centuries [*Mann et al.*, 1998]. The northern high latitudes experience pronounced warming, especially during winter and spring over Alaska, northern Canada, and northern Eurasia [*Hansen et al.*, 1999]. Associated with this high-latitude warming is a reduction in annual snow cover and an

earlier disappearance of snow in spring [*Groisman et al.*, 1994; *Konstantin et al.*, 1999]. These changes have affected the global carbon cycle; the amplitude of the seasonal CO$_2$ cycle in the Northern Hemisphere has increased, on average, by about 30% since the early 1960s [*Keeling et al.*, 1996].

These changes beg the question, can we detect the effect of interannual variations in climate on global biospheric activity. *Myneni et al.* [1997] report that the photosynthetic activity of terrestrial vegetation between 45°N and 70°N increased between 1981 and 1991. Other studies report warming-related phenological changes in plants [*Colombo*, 1998; *Schwartz*, 1998; *Bradley et al.*, 1999; *Menzel and Fabian*, 1999], birds [*Crick and Sparks*, 1999; *Brown et al.*, 1999], and poleward range extensions by birds [*Thomas and Lennon*, 1999] and butterflies [*Parmesan et al.*, 1999].

The importance of vegetation in the global carbon cycle is well known [*Tans et al.*, 1990; *Schimel et al.*, 1996]. The relations among temperature, growth rate of atmospheric CO$_2$, and vegetation activity are a complicated tangle of forcing/feedback responses, often with lag and scale dependencies [*Braswell et al.*, 1997; *Houghton et al.*, 1998]. Evidence for a biotic response to climate change sometimes is based on analyses of satellite-sensed data for the normalized difference vegetation index (NDVI). The NDVI data capture

[1]Department of Geography, Boston University, Boston, Massachusetts, USA.

[2]Biospheric Sciences Branch, NASA Goddard Space Flight Center, Greenbelt, Maryland, USA.

[3]Science Systems and Applications Inc., Biospheric Sciences Branch, NASA Goddard Space Flight Center, Greenbelt, Maryland, USA.

the contrast between red and near-infrared reflectance of vegetation, which signals the abundance and energy absorption by leaf pigments such as chlorophyll. NDVI can be used to proxy the vegetation's responses to climate changes because it is well correlated with the fraction of photosynthetically active radiation absorbed by plant canopies and thus leaf area, leaf biomass, and potential photosynthesis [*Myneni et al.*, 1995]. The data typically are of global extent, 8 km spatial resolution and 10-15 day temporal frequency, with the record beginning in July of 1981 and extending to the present.

Investigations of seasonal changes and interannual variability of global vegetation activity using NDVI assume that changes in NDVI contain clues about the vegetation's response to climate. However, the interannual signal of vegetation canopy reflectance is subtle and subject to nonvegetation effects. Many factors, unrelated to ecosystem structure or function (namely, satellite drift, calibration uncertainties, intersatellite sensor differences, bidirectional and atmospheric effects, volcanic eruptions, etc.), can introduce extraneous variability in NDVI, and this variability can be easily misidentified as real NDVI changes [*Gutman and Ignatov*, 1995; *Privette et al.*, 1995; *Rao and Chen*, 1995; 1996; *Myneni et al.*, 1998; *Gutman*, 1999]. Therefore it is important to develop, test, and apply corrections in order to produce a consistent and calibrated time series for NDVI from the raw satellite data.

Another important caveat is that some time series of climate variables and satellite data are nonstationary; that is, they contain stochastic trends. The presence of stochastic trends means that standard statistical techniques such as ordinary least squares (OLS) may indicate a significant relation among variables when none, in fact, exists. The Intergovernmental Panel on Climate Change notes these difficulties: "rigorous statistical tools do not exist to show whether relationships between statistically nonstationary data of this kind are truly statistically significant..." [*Folland et al.*, 1992]. Despite these difficulties, standard statistical methods are used to investigate the relations among changes in climate variables and ecosystems [e.g., *Braswell et al.*, 1997; *Myneni et al.*, 1997]. The interpretation of these results is clouded by the inability to determine whether relations among nonstationary variables are statistically significant.

Because of the aforementioned problems it is important to characterize and minimize the nonvegetation effects in analyses of NDVI time series, choose statistical techniques appropriate for time series properties of NDVI and climate data, and interpret the results carefully in order to understand the relations between climate variations and vegetation dynamics. With this in mind, we analyze a recently developed NDVI data set to characterize and understand interannual variability in vegetation activity during the past 2 decades. The outline of this article is as follows. Section 2 describes the data sets, methodology, and assessment of NDVI data quality. The changes in NDVI are presented in section 3. The relationship between changes in NDVI and land surface temperature is discussed in section 4, and section 5 presents some concluding remarks.

2. Data and Methods

2.1. GIMMS NDVI Data Set

We use the continental data set at 8 km resolution for the period July 1981 to December 1999 produced by the Global Inventory Monitoring and Modeling Studies (GIMMS) group from the advanced very high resolution radiometers (AVHRR) onboard the afternoon-viewing National Oceanic and Atmospheric Administration's (NOAA) series satellites (NOAA 7, 9, 11, and 14). This data set consists of five subsets: Africa, Australia, North America, South America, and Eurasia. It contains channels 1 (0.58 – 0.68 μm) and 2 (0.73 – 1.1 μm) reflectances, channels 4 (10.3 – 11.3 μm), and 5 (11.5 – 12.5 μm) brightness temperatures, solar and view zenith angles, and the day of compositing. These channel and associated data correspond to the maximum NDVI value during a 15-day compositing period. The infrared data (channels 4 and 5) are not used in this paper and all the corrections and procedures described below refer only to visible, near-infrared (NIR), and NDVI data. The NDVI is expressed on a scale between -1 and +1. GIMMS NDVI ranges between -0.2 and 0.1 for snow, inland water bodies, deserts, and exposed soils, and increases from about 0.1 to 0.7 for increasing amounts of vegetation.

The important data processing features include improved navigation, sensor calibration, and atmospheric correction for stratospheric aerosols. A navigation algorithm that uses an accurate orbit model, the latest available satellite ephemeris and instrument clock correction data is implemented in the GIMMS production system [*Rosborough et al.*, 1994]. This algorithm also accounts for target elevation through the use of a digital elevation model. Calibration of AVHRR visible and NIR measurements is necessary before we can analyze time series that are acquired from four satellites [*Los*, 1993; *Rao and Chen*, 1995; 1996]. A method based on data from high cold clouds and the dark ocean is used to calibrate the data set [*Vermote and Kaufman*, 1995]. However, this calibration is insufficient; the NDVI of desert targets is not sufficiently stable. The calibration is improved by using a sensor degradation correction method by *Los* [1998] to the entire data set. This method provides good sensor degradation and intersatellite calibration. Stratospheric aerosols associated with volcanic eruptions, however, tend to have longitudinally homogeneous distributions within 2 months of injection and then slowly decrease with time. This means that stratospheric aerosols effects must be corrected even in time series of composited data. The GIMMS data from April 1982 to December 1984 and from June 1991 to December 1993 are corrected to remove the effects of stratospheric aerosol loading from El Chichon and Mt. Pinatubo eruptions with a method developed by *Vermote and El Saleous* [1994]. Such correction raises the NDVI values, having a strong effect in the low latitudes and a small effect in the high latitudes.

The surface reflectance measured by satellite sensors is affected by the presence of the atmosphere between the sensor and the target. Ozone and water vapor absorption affect the signal recorded in the visible and NIR channels. Rayleigh scattering mainly affects the visible channels and is more pronounced when dealing with low sun elevations and larger view angles. Aerosol scattering affects both visible and NIR channels. In the AVHRR time series the major problems are with the continuous changes in sensor sensitivity (calibration problem) and with satellite orbital drift, which leads to continuous changes in sun-target-sensor geometry. The orbital drift effect is always combined with the effects of absorption and scattering because of ozone, water vapor, Rayleigh scattering, and aerosols in the atmosphere and surface anisotropy [*Gutman*, 1999]. In general, properties of both surface and atmosphere are spatially and temporally variable;

the sensitivity of visible, NIR and NDVI data and surface bidirectional effects are different to different atmospheric constituents and surface cover types; quantitative characteristics of atmospheric constituents (water vapor, tropospheric aerosols) and surface are insufficient [*Gutman*, 1999]. This makes the problem even more complex. Although there is a large body of research on this topic, successful, operational atmospheric correction, at global and continental scales, remains a challenge because it involves the closure of a system of radiance equations with many more unknowns than measurable quantities. No explicit atmospheric corrections except for correction for stratospheric aerosols are applied to the GIMMS NDVI data set.

However, the above mentioned processing of the GIMMS NDVI data set helps account for drift in sensor sensitivity and introduce corrections to calibration trends. It is also important to note that surface bidirectional effects are most noticeable when atmospheric corrections are made to the top-of-the-atmosphere measurements. That is, to some extent, atmospheric effects and surface bidirectional effects tend to cancel out. These nonvegetation effects can be further minimized, to a large extent, by analyzing only the maximum NDVI value within each 15-day interval. To do so, each month is divided into two compositing periods; days 1-15 are compositing period 1, and days 16 to the end of the month are compositing period 2. The maximum NDVI value during each compositing period is chosen to represent the compositing time period. Over the biweekly periods these data generally correspond to observations in the forward, nearest to nadir view directions and clear atmospheres [*Los et al.*, 1994; *Holben*, 1986]. Maximum value NDVI compositing minimizes, but does not eliminate, residual atmospheric and bidirectional effects. That is why it is important to assess the relation between changes observed in the GIMMS NDVI data set and changes observed in alternate data sets, generally temperature and precipitation. Statistical analysis reported in section 4 does indeed point to meaningful interannual variations in the composited NDVI data set. Further discussion of the GIMMS NDVI quality is described in section 2.4.

2.2. GISS Surface Temperature Data Set

The NASA Goddard Institute for Space Studies (GISS) surface temperature analysis provides monthly measures of global near-surface air temperature since 1880. The data set is derived from measurements taken at rural and small towns. Measurements from urban stations are adjusted so that their long-term trend matches their rural neighbors. The data set used here is gridded global temperature anomalies, with respect to the 1951-1980 mean, from 1981 to 1999 at 2° x 2° resolution. The area-averaged temperature anomaly is more accurate than the area-averaged absolute temperature [*Hansen et al.*, 1999]. The GIMMS infrared temperature data are not used because of problems associated with calibration and lack of required corrections. We believe that the use of an independent temperature data set helps support and verify our results from the GIMMS NDVI data analysis.

2.3. Methodology

2.3.1. Scaling of temperature and NDVI data.
Temperature and NDVI data are reported at different spatial and temporal resolutions. Each sample of 2° x 2° temperature data is considered to be a square cell with a constant

temperature value. For a given NDVI pixel p, its temperature $T(p,c,m,y)$ in composite period c (1 or 2), month m (from 1 to 12), and year y (from 1982 to 1999) is found by projecting its location (longitude and latitude) on the temperature data set. Here $T(p,1,m,y)$ equals $T(p,2,m,y)$ because the temperature data set has a monthly frequency.

2.3.2. Calculating the NDVI and SZA anomalies.
The NDVI and solar zenith angle (SZA) data display significant and relatively constant intra-annual seasonality. This pattern is not relevant to data quality assessment and the analysis of interannual variation. Therefore the seasonality is removed from the data as follows. Let $X(p,c,m,y)$ be the NDVI or SZA of pixel p, composite c, month m, and year y. The average annual cycle is defined as

$$\bar{X}(p,c,m) = \frac{1}{N_y}\sum_{y=82}^{99} X(p,c,m,y),\qquad(1)$$

where N_y is the number of years ($N_y = 18$). The anomaly $X'(p,c,m,y)$ is calculated as

$$X'(p,c,m,y) = X(p,c,m,y) - \bar{X}(p,c,m).\qquad(2)$$

Annual averaging and anomaly calculations are performed only over pixels that satisfy certain conditions, which are discussed in section 2.4.

2.3.3. Spatial and temporal averaging of NDVI/SZA and temperature data.
Because of the large number of pixels in the satellite data set, aggregation in space and/or time is necessary. For a given region or latitudinal band, let N_t be the total number of pixels of interest, and $X''(p,c,m,y)$ represent either $T(p,c,m,y)$, $X(p,c,m,y)$, or $X'(p,c,m,y)$ as defined in section 2.3.1 and 2.3.2. The spatial average $X_s(c,m,y)$ is calculated as

$$X_s(c,m,y) = \frac{1}{N_t}\sum_{p=1}^{N_t} X''(p,c,m,y).\qquad(3)$$

Two types of temporal averages (monthly or yearly) with two different types of data, a single-pixel time series $X''(p,c,m,y)$ or a spatially averaged time series $X_s(c,m,y)$ are used in the following analyses. For a given period, let N_m (N_y) be the total pixels in month m (year y), the temporal average $\bar{X}_t(c,m)$, $\bar{X}_t(c,y)$, $\bar{X}_t(p,c,m)$ and $\bar{X}_t(p,c,y)$ are calculated as

$$\bar{X}_t(c,m) = \frac{1}{N_y}\sum_{y=1}^{N_y} X_s(c,m,y),\qquad(4)$$

$$\bar{X}_t(c,y) = \frac{1}{N_m}\sum_{m=1}^{N_m} X_s(c,m,y),\qquad(5)$$

$$\bar{X}_t(p,c,m) = \frac{1}{N_y}\sum_{y=1}^{N_y} X''(p,c,m,y),\qquad(6)$$

$$\bar{X}_t(p,c,y) = \frac{1}{N_m}\sum_{m=1}^{N_m} X''(p,c,m,y).\qquad(7)$$

Again, we emphasize that spatial and temporal averaging is performed only over pixels that satisfy certain conditions, which are discussed in section 2.4, section 3, and section 4.

2.3.4. Spatial autocorrelation.
We analyze the data for spatial autocorrelation to evaluate the spatial pattern of NDVI changes and assess the quality of the GIMMS NDVI data set. Strong spatial autocorrelation means that NDVI changes of

adjacent pixels are more similar than would be generated by a random process. The degree of spatial autocorrelation can reflect three underlying processes. If changes in NDVI are due to artifacts such as satellite drift, sensor degradation, and intersatellite difference, we would expect a high degree of spatial autocorrelation and the changes in NDVI would have the same sign over the same biome or latitudinal band [*Myneni et al.*, 1998; *Gutman*, 1999], especially in the northern high latitudes. If NDVI variations are dominated by a randomly distributed (in space) nonvegetation effect such as soil background influence, we would expect pixels to show differences in NDVI variations over small geographical areas. If changes in NDVI are generated by changes in climate, for example, temperature, we would expect a high degree of spatial autocorrelation, but the sign associated with the NDVI changes would vary among regions.

To calculate a simple measure for the spatial autocorrelation of NDVI changes, we classify pixels between two categories: "1" for high NDVI increase and "0" for low NDVI increase or NDVI decrease (details in section 3.2). For a given region we test whether the spatial arrangement of 1/0 is "clustered," "dispersed," or "random." If the 1/0 values are scattered randomly over the region, there will be no spatial autocorrelation. To test the significance of spatial autocorrelation, it is necessary to know the probability that the observed number of 1/0 joints occur by chance. This probability can be estimated from the mean and standard deviation for the case of a random pattern [*Ebdon*, 1985]. The expected number of 1/0 joints, E_{bw}, is defined by

$$E_{bw} = \frac{2JBW}{N(N-1)}, \qquad (8)$$

where J is the total number of 1/0 joins, B is the number of "1" areas, W is the number of "0" areas, and N is the total number of areas in the study region ($N=B+W$). The standard deviation of E_{bw} is given by

$$\sigma_{bw} = \sqrt{E_{bw} + \frac{\sum L(L-1)BW}{N(N-1)} + p_1 - E_{bw}^2},$$

$$p_1 = \frac{4[J(J-1) - \sum L(L-1)]B(B-1)W(W-1)}{N(N-1)(N-2)(N-3)}, \qquad (9)$$

where L is the number of 1/0 joints between a given grid and its contiguous grids. The null hypothesis that the spatial arrangement of "1" (high NDVI increase) is random is tested with a Z statistic, which follows a normal distribution and is calculated as

$$Z = \frac{O_{bw} - E_{bw}}{\sigma_{bw}}, \qquad (10)$$

where O_{bw} is the observed number of 1/0 joints.

The critical value of the Z statistic at 5% (1%) significance level is 1.96 (2.58). If the calculated Z values are greater than the critical value, we can reject the null hypothesis, and we can say that the observed arrangement of "1" is said to be "significantly clustered (dispersed)" at the 5% (1%) level; otherwise, it is said to be "random."

2.4. Assessment of GIMMS NDVI Data Quality

Despite the corrections described in section 2.1, the NDVI of GIMMS data set may still contain variations due to orbital

drift and incomplete corrections for calibration loss and atmospheric effects. Especially, as the corrections for changes in sun-target-satellite geometry are not explicitly made in the GIMMS data processing, variations due to orbital drift should be expected. The effects for NDVI variations are weak, but not necessarily negligible [*Gutman*, 1999]. Empirical and theoretical analyses indicate that NDVI is minimally sensitive to changes in SZA due to orbital drift and sensor changes, and this sensitivity decreases as leaf area index increases [*Kaufmann et al.*, 2000]. The SZA effect is large for reflectance in the red and NIR channel but is indeed weak for NDVI. Ground observations over boreal forests also indicate that changes in SZA have little effect on the seasonal NDVI pattern [*Huemmrich et al.*, 1999]. The magnitude of these nonvegetation effects is discussed next.

The residual nonvegetation effects are expected to be largest and best seen over a bright barren surface [*Kaufmann et al.*, 2000], such as the Sahara, because the reflectivity does not change over time [*Tucker et al.*, 1994]. We analyze a large arid region in the Sahara (3°W-16°E; 20°N-26°N) of 19,076 pixels (1.22 x 10^6 km^2) for the presence of variations due to orbital drift and incomplete corrections. GIMMS NDVI and SZA anomalies are produced by averaging all Sahara pixels using the method outlined in section 2.3.2. For comparison, we simulate the NDVI of this region with a radiative transfer model [*Jacquemoud et al.*, 1992], ignoring the atmospheric effects and using time-invariant optical and structural properties of a dry sandy soil together with the actual time series of SZA at the time of satellite measurements over this area. The parameters used in this model include (1) view angle, 0; (2) roughness parameter, h=0.109; (3) phase function parameters, b=1.642, c=0.731, b'=0.317, and c'= -0.025; and (4) single scattering albedo, ω=0.5869 for the red band (0.58-0.68 µm) and ω=0.6989 for the near-infrared band (0.725-1.1 µm). These two ω are generated by averaging soil particulate single scattering albedo spectrum given by *Jacquemoud et al.* [1992] over the corresponding wavelength bands. The simulated NDVI time series is used to assess NDVI variations with respect to SZA changes only.

Figure 1a shows the time series of GIMMS NDVI, modeled NDVI, and SZA. Spectral methods, such as the singular spectrum analysis (SSA), can be used to isolate periodic and trend components, oscillations, and other structured components [*Vatuard et al.*, 1989]. We use the SSA toolkit [*Dettinger et al.*, 1995] to decompose each of these time series into eight statistically independent components by accounting for the lag covariance structure. The time series reconstructed with the first (second) component, shown in Figure 1b (Figure 1c), capture 6% (6%), 60% (23%), and 60% (23%) of the total variances of the original time series, respectively. Reconstructions with higher components, which capture a successively smaller percentage of the total variance, are not shown for brevity. The modeled NDVI has the same variance structure as SZA, which indicates that SZA has a significant effect on the NDVI for bare ground. Had the calibration and corrections in the production of GIMMS NDVI been ineffective or incomplete, the variance structure of GIMMS NDVI series would resemble either that of the modeled NDVI or the SZA time series. The dissimilarity in the variance distribution of all reconstructed components between the GIMMS NDVI and modeled NDVI shows that the methods used to generate the GIMMS NDVI data set largely minimized the SZA effects,
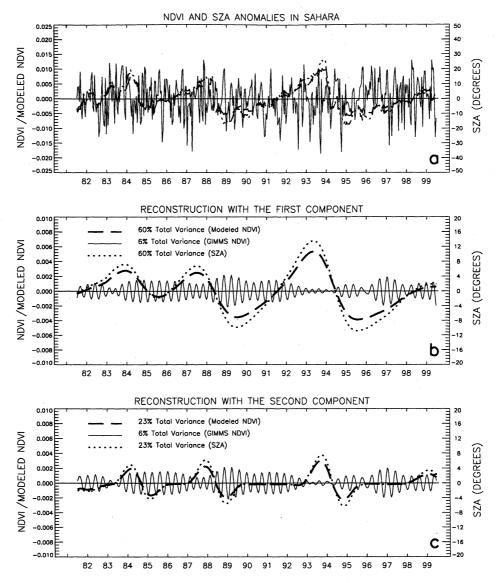
Figure 1. Spectral analysis of the time series of NDVI and solar zenith angle (SZA) anomaly from the Sahara (3°W-16°E; 20°N-26°N): (a) original time series, (b) reconstruction with the first component, and (c) reconstruction with the second component. The GIMMS NDVI, modeled NDVI, and SZA series are solid, dashed, and dotted lines, respectively.

based on the condition that there is no trend in the atmospheric constituents, especially water vapor and aerosols. A major feature of GIMMS NDVI series is its stability, without apparent discontinuities between satellites and no significant systematic variations during the period of any one satellite. Although the observed low-magnitude high-frequency variations still show clues of individual satellites, such signal is weak and its magnitude is very small, indicating the random nature of small variations due to the SZA and atmospheric effects over bare stable targets, such as the Sahara.

On the basis of the assumption that deserts act as a stable target, any trends in the GIMMS NDVI for the desert can be attributed to calibration, orbital drift, and atmospheric and bidirectional effect residuals. Linear trends estimated from the GIMMS NDVI time series for the Sahara (Figure 1) are 0.00027 yr^{-1} (NOAA 7), -0.00064 yr^{-1} (NOAA 9), 000286 yr^{-1}

(NOAA 11), and 0.000526 yr^{-1} (NOAA 14). All estimates are extremely small and none is statistically significant even at the 0.2 level. We note a positive estimate for the NOAA 14 period, as given by *Gutman* [1999] for the case of the global vegetation index (GVI) data set, but its magnitude is insignificant compared with the GVI estimate. *Gutman* [1999] assumed that tropical humid forests also could be used as a stable target to assess the GVI data set. Because of the possibility of influences from El Niño-Southern Oscillation (ENSO) [*Myneni et al.*, 1996; *Asner et al.*, 2000] (signal) and residual clouds (noise) and saturation problems over dense vegetation, the NDVI data from tropical humid forests are not used as a stable target. Instead, we use the land surface temperature observations, an independent data set, to support and verify our results from GIMMS NDVI data analysis (section 4).

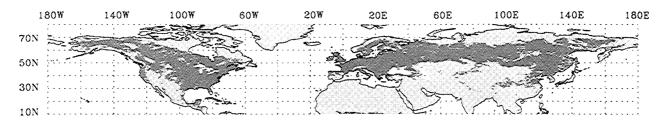We must realize limitations associated with using the

Figure 2. Map of vegetated pixels (solid) used in this study. Vegetated pixels are identified as those with (1) June to August NDVI composite values > 0.1 for all years and (2) June to August average NDVI values > 0.3 for all years.

Sahara desert to demonstrate the NDVI data quality over high-latitude vegetated surfaces. Different changes in the atmospheric constituents and sun-target-satellite geometry may introduce different NDVI variations over the two surface types, but it is difficult to find another stable target in the high latitudes. Therefore time series of NDVI anomalies for different latitudinal bands in the northern high latitudes are analyzed next to assess those nonvegetation signals.

To reduce any remaining nonvegetation effects on NDVI, and to exclude snow, barren, and sparsely vegetated areas, we analyze relatively dense vegetated pixels only. This also reduces the sensitivity of NDVI to SZA changes [*Kaufmann et al.*, 2000] and excludes artifacts due to temporal variations in ground reflectivity in sparsely vegetated areas. We define "vegetated pixels" as those with (1) June to August NDVI composite values > 0.1 in all years and (2) June to August
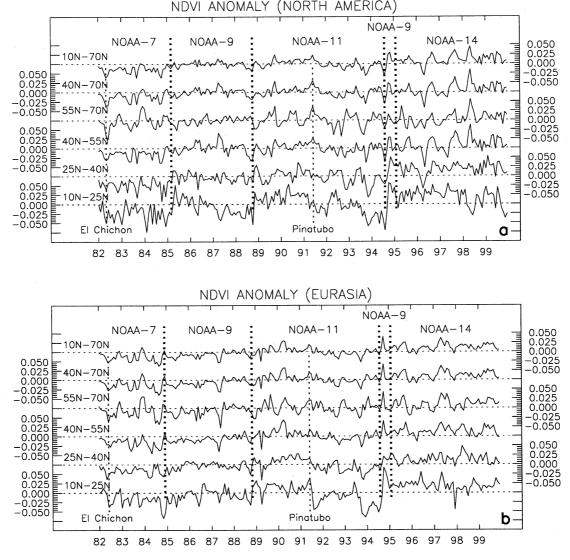

Figure 3. Time series of spatially averaged NDVI anomaly for different latitudinal bands of (a) North America and (b) Eurasia.

average NDVI values > 0.3 for all years. The resulting vegetation mask (Figure 2) compares well with other land cover maps [*DeFries et al.*, 1998]. This mask also ensures that data from the same pixels are utilized in the entire analysis, unlike *Myneni et al.* [1997].

Time series of NDVI anomalies for different latitudinal bands in North America and Eurasia are generated by spatially averaging over all vegetated pixels with composite NDVI values > 0.1 (Figure 3). The anomalies for the tropics (10°N-25°N) exhibit large fluctuations, associated with satellite changes, orbital drift, volcanic eruptions, and possibly ENSO influences. There are few vegetated pixels located in this zone. This is consistent with theoretical and statistical analyses which indicate that the impact of sensor changes and orbital drift increases with decreasing leaf area [*Kaufmann et al.*, 2000].

The data series 10°N-70°N resembles the 40°N-70°N series because the dominant signal from both continents of the Northern Hemisphere is generated by the dense temperate and boreal vegetation. The dramatic loss of orbit in the case of NOAA 11 is particularly evident in the data from the tropics (10°N-25°N). GIMMS uses data from NOAA 9 for the period between NOAA 11 and NOAA 14, and this creates a clear discontinuity in the data series. It is interesting to note that the impact of El Chichon aerosols on NDVI, immediately after the eruption in May 1982, is stronger in the North American data than in the Eurasian data. Similarly, the impact of Mt. Pinatubo is stronger in the Eurasian data than in the North American data.

The downward trend in NDVI for all latitudes from mid-1991 onward coincides with the weak 1991-1992 El Niño event and eruption of Mt. Pinatubo, which brings into question the efficacy of stratospheric aerosol corrections. The uncorrected values are lower than the corrected data. For example, the corrected (uncorrected) May to September average NDVI values for the 40°N-45°N latitudinal band from 1991-1993 are 0.460 (0.455), 0.455 (0.435), and 0.462 (0.460), respectively. To check their accuracy, we compare the aerosol optical depths retrieved from the image data with those from the Stratospheric Aerosol and Gas Experiment instrument [*Sato et al.*, 1993] and other published estimates. Several reprocessings of the data indicate that NDVI decreases from 1991 to 1992. Moreover, the stratospheric aerosol optical depths required for NDVI to increase from 1991 to 1992 are inconsistent with all estimates of observed and retrieved aerosol optical depths. Therefore we believe that NDVI decreased from 1991 to 1992, possibly because of the cooling that followed the eruption of Mt. Pinatubo [*Hansen et*

al., 1996]. The relation between NDVI and land temperature in the northern high latitudes is investigated in section 4.

3. NDVI Changes in North America and Eurasia

The results outlined in section 2.4 indicate that the nonvegetation variations in NDVI for North America and Eurasia have been minimized from the GIMMS NDVI data set. In general, NDVI increases over time in the northern high latitudes, and this increase is concentrated spatially in a way that suggests that the GIMMS NDVI data measure changes in vegetation.

3.1. Trends in Spatially Averaged NDVI Between 40°N and 70°N
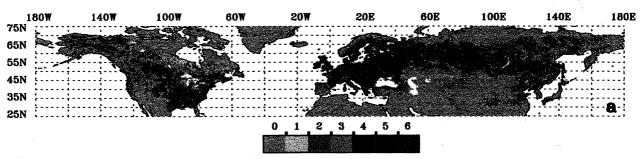
The upward trend in the time series of NDVI between 40°N and 70°N (Figure 3) is a characteristic feature of recent interannual variations in vegetation activity of the north [*Myneni et al.*, 1997]. Linear time trends in NDVI estimated by OLS, for spring (April to May), summer (June to August), autumn (September to October), and the growing season (April to October) in vegetated areas between 40°N-70°N are given in Table 1. From 1982 to 1999, NDVI in Eurasia (North America) increases by 20.87% (16.84%) in spring, 8.73% (5.17%) in summer, 15.06% (9.67%) in autumn, and 12.41% (8.44%) during the growing season. All NDVI trends except spring in North America are statistically significant at the 5% level. The absolute and percent NDVI changes are largest during spring in both continents. Likewise, all Eurasian trends are larger than North American trends. Seasonal differences in these trends and their statistical significance are tempered by the possibility that the NDVI data contain a stochastic trend. In that case, none of the trends in Table 1 may be significant at the 5% level.
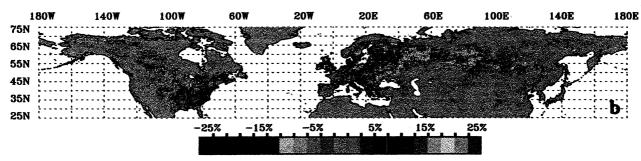
3.2. Spatial Pattern of NDVI Trends

We use three methods to illustrate spatial patterns of NDVI change during the growing season. First, we define an index of persistence as follows. Linear trends in growing season average NDVI are calculated for the periods 1982-1987, 1982-1989, 1982-1991, 1982-1993, 1982-1995, 1982-1997, and 1982-1999. We denote these trends as $t(i)$, i = 1, 2, ..., 7. A score of 1 is given if $t(i+1)$ > 80% of $t(i)$; otherwise the score is zero. The sum of these scores is calculated as an index of persistence. The maximum possible score is 6. This index can identify regions where NDVI has increased consistently, as opposed to a trend estimate, which in the case of a small sample can be biased by outliers. A persistence index of 5 or more, which shows a pixel where NDVI has increased in five or six of the six periods, is termed "high persistence," while "low persistence" refers to a pixel with persistence index between 1 and 4. Second, we identify pixels that have a linear trend in NDVI over the 18-year period that is statistically significant at the 5% level. Third, NDVI changes are presented as the difference between the last 5 years (1995-1999) and the first 5 years (1982-1986). The resulting maps of NDVI spatial changes are shown in Plate 1, together with climatological NDVI which shows the pattern of vegetation in the north.

The changes in NDVI measured by these three methods are roughly consistent. Pixels with high persistence, colored red
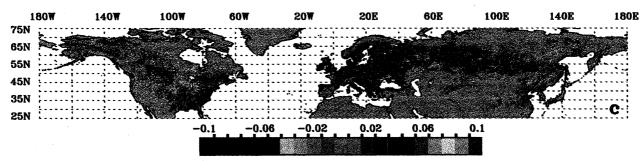
Table 1. NDVI Trends Between 40°N and 70°N in Eurasia and North America From 1982 to 1999[a]

Season	NDVI Changes in 18 Years		
	Absolute Values	Percent (%)	t Statistic
April-May (EA)	0.047	20.87	3.56[b]
April-May (NA)	0.039	16.84	1.96
June-August (EA)	0.042	8.73	8.01[b]
June-August (NA)	0.025	5.17	3.47[b]
September-October (EA)	0.043	15.06	3.91[b]
September-October (NA)	0.031	9.67	2.85[b]
April-October (EA)	0.044	12.41	6.53[b]
April-October (NA)	0.031	8.44	3.64[b]

[a]EA, Eurasia; NA, North America.
[b]Statistically significant at the 0.05 level.

ZHOU ET AL.: VEGETATION RESPONSE TO GLOBAL WARMING

Plate 1. Spatial patterns of (a) persistence in NDVI increase, (b) NDVI trend at 5% significance level, (c) NDVI difference between 1995-1999 and 1982-1986 averages, and (d) climatological NDVI from July 1981 to December 1999, during the growing season defined as April to October months.

and purple in Plate 1a, also are pixels where NDVI shows a statistically significant trend (Plate 1b) and large increase (Plate 1c) over the sample period. The pattern of high persistence and large increases in NDVI are especially noteworthy in boreal Eurasia, along a broad swath of land east of 25°E and north of 50°N. This region includes the grasslands and croplands of the south central Russian uplands and extends northeast through the unmanaged mixed and needle forests to the Bolshezemalskaya Tundra. East of the Urals, there is a contiguous region of high persistence over the west Siberian plain and the central Siberian plateau. East of Lake Baikal, there is a band of pixels which displays high persistence and a large NDVI increase between 50°N and 55°N and that extends east to the Aldan plateau. These regions in Siberia and eastern Russia consist mostly of natural forests with arctic grasses and tundra to the north. Outside of this broad swath, large regions of densely vegetated areas in central Europe and Sweden also are notable. About 78% (9.8×10^6 km²) of the vegetation in these regions between 40°N and 70°N is unmanaged [*DeFries et al.*, 1998], and almost 58% (7.3×10^6 km²) is forests and woodlands, an area equivalent to about 78% of the USA. The regions of high persistence in Eurasia are also regions of high average growing season NDVI (Plate 1d). The degree of spatial coherence seen in Eurasia, i.e., large areas of high persistence circumscribed by regions of low persistence, is absent in North America. There, pixels with high persistence are relatively fragmented, and the densely vegetated temperate and boreal forest regions in North America do not show a noteworthy pattern. Pixels with high persistence and significant NDVI increases in North America are located mainly in the needle forests of the southeast and grasslands of the upper Midwest. In total, only about 30% of the vegetated pixels between 40°N and 70°N in North America display high persistence, compared with more than 61% of the vegetated area in Eurasia. On the other hand, NDVI values in the boreal vegetation in Alaska, Canada, and northeastern Asia (east of 95°E and north of 40°N) decrease between the last 5 years and the first 5 years (Plate 1c). In these areas the decline is especially apparent in the summer period, and a higher proportion of vegetated pixels show NDVI decrease in North America than in Eurasia (figure not shown for brevity). Possible reasons for this decline are discussed in section 4.

We test the null hypothesis that the spatial distribution of pixels with high persistence in Plate 1a is random in North America and Eurasia. The calculated *Z* values for Eurasia and North America are -161.95 and -96.59, respectively. Both exceed the critical value 2.58 at the 1% significance level. This implies that it is highly unlikely that a random process generated the spatial pattern of high persistence in NDVI shown in Plate 1a. In other words, pixels with high persistence are significantly clustered. This can be seen from Plate 1a in which all red or purple pixels (high persistence) are clustered around some regions, although these regions are more scattered in North America than in Eurasia. As discussed in section 2.3.4, there are three possible spatial patterns of NDVI changes. The observed spatial pattern of NDVI changes (Plate 1a) and observed NDVI decrease in some areas (Plate 1c) reduce the likelihood that NDVI increase is due to artifacts because we do not see the similar NDVI changes in the same biome or latitudinal band in the high latitudes on both continents. The result of the

autocorrelation analysis also reduces the likelihood that the changes in NDVI are caused by a spatially random process. The observed spatial patterns of NDVI changes in Plate 1a are consistent with the notion that these NDVI changes are associated with changes in climate (for example, temperature), that tend to occur over large geographic areas. Nonetheless, it is possible that some portion of NDVI variations is caused by nonvegetation effects. To analyze these results further, we use an independent climate data set, temperature, to support our analyses of GIMMS NDVI (section 4).
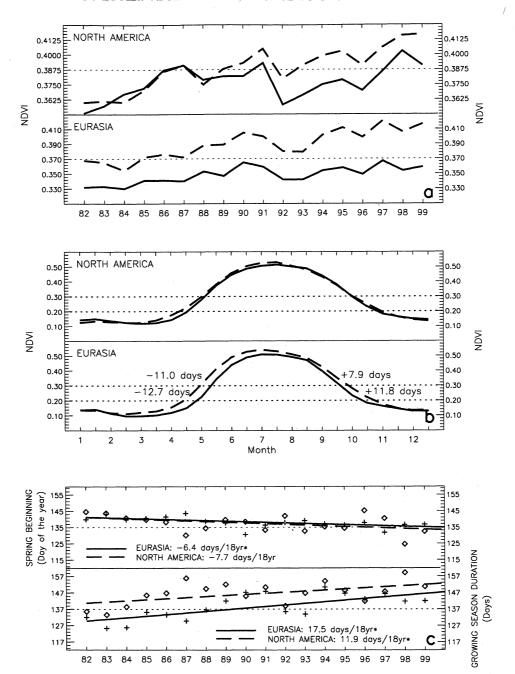
3.3. Growing Season Changes

The annual integral of NDVI is a proxy for vegetation photosynthetic activity over the entire growing season [*Fung et al.*, 1987]. This activity can be characterized by the two dimensions of the area under the seasonal NDVI curve; its magnitude and growing season duration. An increase in either or both can generate photosynthetic gains [*Randerson et al.*, 1999].

First, we define the growing season as April to October and assess changes in the magnitude of growing season NDVI average between 40°N and 70°N from 1982 to 1999 (Figure 4a), where the time series from pixels with high persistence and low persistence are shown. Pixels of high persistence (low persistence) in Eurasia and North America show NDVI increases of about 9%-16% (4%-12%). In Eurasia the average NDVI of pixels with high persistence (0.389 ± 0.019) is greater than that of pixels with low persistence (0.348 ± 0.011). In North America the average NDVI values of these two types of pixels are comparable.

Second, we define growing season as the number of days with NDVI greater than a threshold value and assess the changes in the duration of photosynthetic activity. The seasonal course of NDVI (averaged over the 18.5 years of data record) in Eurasia differs between pixels with high persistence and low persistence (Figure 4b). The duration of active growing season increases by about 19-24 days in Eurasia compared with about 4-12 days in North America, depending on the threshold value. We also investigate changes in growing season duration by tracking changes in the timing of spring greening (when the seasonal NDVI rises above a threshold value) and end of activity in autumn (when the seasonal NDVI curve drops below a threshold value). For example, using a threshold value of 0.3, the beginning of spring advanced by about 8 ± 4 days in North America and 6 ± 2 days in Eurasia from 1982 to 1999 (Figure 4c). Similarly, the termination of activity in autumn was delayed by 4 ± 3 days in North America and 11 ± 3 days in Eurasia. Therefore the duration of the active growing season increased by about 12 ± 5 days in North America and 18 ± 4 days in Eurasia. The fact that the estimated growing season duration from two methods (Figure 4b versus 4c) shows a large difference in Eurasia relative to North America lends further credence to the pervasive and unfragmented nature of NDVI changes in Eurasia.

Several previous studies note an extension in the growing season duration, primarily due to an early spring [*Keeling et al.*, 1996; *Myneni et al.*, 1997; *Colombo*, 1998; *Schwartz*, 1998; *Menzel and Fabian*, 1999; *Bradley et al.*, 1999]. Our data support the idea of an early spring, but we also observe a
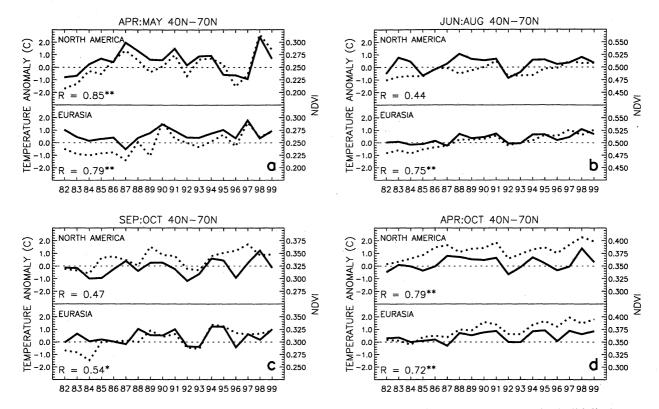
Figure 4. Changes in the seasonal NDVI magnitude and duration between 40°N and 70°N from pixels with high persistence (persistence indices between 5-6; dashed line) and low persistence (persistence indices between 1-4; solid line) in Eurasia and North America: (a) April to October average NDVI, (b) NDVI annual cycle averaged over 1981-1999. The duration of the active growing season is estimated as the number of days with NDVI values above a certain threshold. (c) Changes in the timing of spring greening and growing season duration estimated as the number of days with NDVI values above a threshold of 0.3 for vegetated areas in the 40°N-70°N band. The solid (dashed) line is the trend estimated by a linear regression for Eurasia (North America). The asterisk denotes statistical significance at the 5% level.

comparable delay in the decline of autumn activity in Eurasia (Figure 4b and 4c). Although consistent with previous results, our results must be interpreted with caution. Measuring the growing season duration requires precise information about the time of spring greening and the end of activity in autumn. We measure the duration of the growing season from data with a coarse temporal resolution (15 days). Our results will change depending on the threshold used to define the growing season and the frequency of the compositing period.

Therefore we emphasize the general changes suggested by the data but not the magnitudes.

4. Consistency Between Changes in NDVI and Temperature Anomaly

Another way to determine whether the changes in NDVI reflect differences in biological activity between North America and Eurasia is to test whether the changes in NDVI

Figure 5. Spatially averaged NDVI (dotted line) and near-surface air temperature anomaly (solid line) between 40°N and 70°N: (a) April to May, (b) June to August, (c) September to October, and (d) April to October. "R" is the correlation coefficient. The double asterisk (single asterisk) denotes the statistical significance at the 1% (5%) level.

are correlated with factors known to affect biological activity. Although not the only, or most important, determinant of biological activity, temperature is an important determinant. If changes in biological activity are responsible for the temporal changes and continental differences in the NDVI data set, they should be correlated with temporal changes and continental differences in ground-based measurements of temperature.

During the past 18.5 years, satellite NDVI data in the northern high latitudes show an increasing trend, but such trends are different for North America and Eurasia. Ground-based meteorological measures of temperature indicate that global surface temperature in 1998 is the warmest in the instrumental record [*Hansen et al.*, 1999]. The rate of temperature change was higher in the past 25 years than during any previous period. The northern latitudes (23.6°N-90°N) have warmed by about 0.8°C since the early 1970s, but not all areas have warmed uniformly. The warming rate in the United States is smaller than in most of the world, and there is a slight cooling trend in the eastern United States over the past 50 years [*Hansen et al.*, 1999].

The time series for NDVI and land temperature anomaly between 40°N and 70°N are generated by spatially averaging over all vegetated pixels with composite NDVI values > 0.1. On both continents, NDVI is positively correlated with the temperature anomaly during spring and the growing season at the 1% significance level (Figure 5). The correlations are weaker during summer and autumn, but are still significant at the 5% level in Eurasia but not in North America.

These regression results must be interpreted carefully. Standard statistical methods are based on the assumption that

the time series are stationary; that is, the mean and variance are constant over time, and the covariance between two time periods depends only on the distance or lag between the time periods. The NDVI and/or surface temperature series may contain stochastic trends and therefore be nonstationary [*Kaufmann et al.*, 2000]. These time series properties violate the assumptions that underline standard regression techniques such as ordinary least squares (OLS), which generate efficient estimates of the relation between stationary variables but tend to overstate the statistical significance of the relation between variables with a stochastic trend. Such relations are termed "spurious regressions" [*Granger and Newbold*, 1974]. When evaluated against standard distributions, the correlation coefficients and t statistics for a spurious regression are likely to indicate that there is a significant relation among variables when, in fact, no relation exists.

One way to avoid a spurious association is to include a deterministic variable in the regression. This has the effect of detrending the original time series. To estimate the relation between NDVI and temperature, we estimate the regression model

$$Y = \beta_0 + \beta_1 X + \beta_2 \text{ time} + \varepsilon, \qquad (11)$$

where Y is the dependent variable, time is the deterministic variable, X is the independent variable, β_0, β_1 and β_2 are regression coefficients, and ε is a stochastic error term. This specification is acceptable only if the dependent variable contains a deterministic trend; if the dependent variable contains a stochastic trend, detrending will introduce errors. Unfortunately, it is difficult to differentiate between deterministic and stochastic trends [*Nelson and Plosser*, 1982;

Table 2. Relationship Between NDVI and Temperature Anomaly in Eurasia and North America From 1982 to 1999[a]

Season	Y	X	$Y = \beta_0 + \beta_1 X + \beta_2 \text{ time} + \varepsilon$			$\Delta Y = \beta_0 + \beta_1 \Delta X + \varepsilon$	
			R^2	β_1	t Statistic	R^2	t Statistic
April-May	EA NDVI	EA T	0.810	0.027	5.383[b]	0.611	4.849[b]
April-May	NA NDVI	NA T	0.828	0.023	7.422[b]	0.648	5.256[b]
April-May	EA NDVI	NA T	0.481	-0.005	-1.054	0.146	-1.603
April-May	NA NDVI	EA T	0.336	-0.021	-1.790	0.091	-1.226
April-May	EA NDVI	NA NDVI	0.209	-0.205	-0.527	0.006	-0.297
April-May	EA T	NA T	0.310	-1.058	-2.523[c]	0.091	-1.224
June-August	EA NDVI	EA T	0.861	0.012	2.563[c]	0.173	1.775[c]
June-August	NA NDVI	NA T	0.524	0.007	1.732	0.176	1.792
September-October	EA NDVI	EA T	0.647	0.014	2.587[c]	0.275	2.386[c]
September-October	NA NDVI	NA T	0.423	0.008	1.496	0.105	1.324
April-October	EA NDVI	EA T	0.917	0.020	5.834[b]	0.752	6.735[b]
April-October	NA NDVI	NA T	0.756	0.016	4.306[b]	0.531	4.120[b]
April-October	EA NDVI	NA T	0.751	0.005	1.210	0.005	0.272
April-October	NA NDVI	EA T	0.493	0.008	1.085	0.121	1.435
April-October	EA NDVI	NA NDVI	0.548	0.528	1.775	0.086	1.188
April-October	EA T	NA T	0.193	0.515	1.464	0.121	1.435

[a]NDVI, spatial average of NDVI for vegetated areas between 40°N and 70°N; T, spatial average of near surface air temperature anomalies (base period 1951-1980) [Hansen et al. 1999] for vegetated areas between 40°N and 70°N; EA, Eurasia; NA, North America.
[b]Statistically significant at the 0.01 level.
[c]Statistically significant at the 0.05 level.

Enders, 1995]. The Dickey-Fuller test statistic [*Dickey and Fuller*, 1979] can be used to detect a stochastic trend but cannot be used reliably here because of short sample period (18 observations). To reduce the likelihood of a spurious regression, we also estimate the following regression model,

$$\Delta Y = \beta_0 + \beta_1 \Delta X + \varepsilon, \qquad (12)$$

in which ΔY and ΔX are the first differences of X and Y, and $\beta_0, \beta_1,$ and ε are as in (11).

The base periods used for deriving NDVI and temperature anomalies are different. This does affect the intercepts in the regression equations, but not the slopes and thus the results and conclusions about the temperature-NDVI relationship discussed below.

Results of regression between the NDVI and temperature anomaly are shown in Table 2. The t statistic is used to test the null hypothesis that the regression coefficient associated with the temperature (β_1) is zero at a predetermined level of significance. The t statistic results for equation (11) and (12) indicate that there is a statistically meaningful relation, at the 1% significance level, between the NDVI and temperature anomaly in the spring and growing season for both Eurasia and North America. A similar relation exists for summer at the 1% significance level and for autumn at the 5% significance level in Eurasia, but not in North America.

The possibility that the relation between NDVI and temperature indicated by equations (11) and (12) is spurious is evaluated further by estimating the relation between Eurasian NDVI and North American temperature or North American NDVI and Eurasian temperature. There is no physical reason to believe that temperature in one continent will affect NDVI in the other continent, and so regression results which indicate a relation will imply that the results described above are spurious. In all cases, the t statistics fail to reject the null hypothesis that the regression coefficients that measure the relation between changes in North America and Eurasia are zero. These results reinforce the conclusion that there is a statistically meaningful relation between temperature anomaly and NDVI within North America and Eurasia.
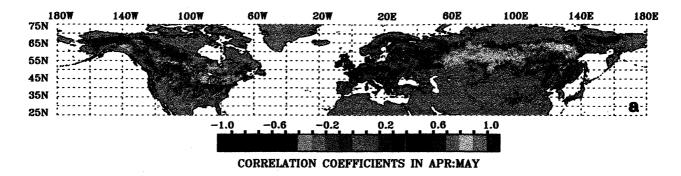
Finally, the possibility that the relation between NDVI and temperature is spurious is investigated by estimating their correlation at a finer spatial scale. We analyze data for spring and the growing season because these relations are statistically significant at the continental scale. NDVI data for individual pixels are spatially aggregated to quarter degree grids and temporally averaged. These averages include data from quarter degree grid cells in which more than 50% of the 8 km pixels are vegetated. In general, the correlation between NDVI and temperature is significant at the 5% level in regions north of 40°N for spring (Plate 2a) and north of 50°N for the growing season (Plate 2b). The areal extent of grids where the correlation coefficient exceeds the 5% threshold is greater in spring relative to the growing season. Together with previous results, we conclude that there is a statistically meaningful relation between GIMMS NDVI and land surface temperature anomaly. Nonetheless, this relation is incomplete because it ignores the other determinants of photosynthetic activity and therefore, may not be consistent with the effect of temperature in areas where other factors limit plant growth. For example, in semiarid regions, precipitation may be a more important factor than temperature [*Myneni et al.*, 1996].

We observe NDVI decreases in some regions (Plate 1). Such a decrease is especially apparent during summer in most of the boreal forest regions of Alaska and Canada (figure not shown for brevity). There is a negative correlation between NDVI and land temperature anomaly during summer in these regions, but the relation is insignificant. This decoupling between NDVI and temperature may be associated with drought, as these regions experienced a pronounced warming [*Hansen et al.*, 1999] without a concurrent increase in growing season precipitation. Tree ring records indicate that temperature-induced drought in the interior of Alaska has disproportionately affected the most rapidly growing white spruce [*Barber et al.*, 2000]. This suggests that drought may limit carbon uptake in a large portion of the North American boreal forest

The proceeding results suggest that warmer temperatures may have promoted plant growth in the north during the
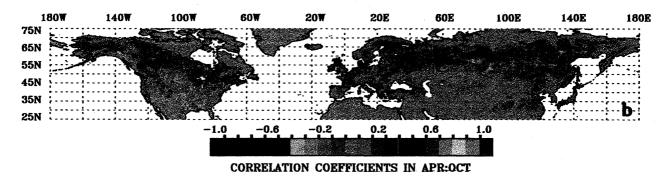
Plate 2. Spatial pattern of the relation between NDVI and near-surface air temperature: (a) correlation for April to May period, (b) correlation for April to October period. The majority of pixels, colored red and purple, are statistically significant at the 5% level.

1980s and 1990s, but this simplistic explanation may be valid only at coarse spatial scales. Possibly it is not mechanistically viable for all northern ecosystems and needs to be refined to allow for lags in the relation between plant growth and temperature induced by biogeochemical feedbacks [*Braswell et al.*, 1997; *Houghton et al.*, 1998]. Further reconciliation between empirical observations that suggest the effect of disturbance [*Zimov et al.*, 1999], soil temperature [*Grace and Rayment*, 2000; *Valentini et al.*, 2000], and winter and summer precipitation [*Vaganov et al.*, 1999; *Barber et al.*, 2000] on plant growth in the north and inferences from satellite [*Myneni et al.*, 1997] and atmospheric CO_2 data [*Keeling et al.*, 1996] also is required.

5. Concluding Remarks

The northern latitudes (23.6°N-90°N) have warmed by about 0.8°C since the early 1970s, but not all areas have warmed uniformly [*Hansen et al.*, 1999]. There is warming in most of Eurasia, but the warming rate in the United States is smaller than in most of the world, and a slight cooling trend is observed in the eastern United States over the past 50 years.

Results of a newly developed satellite vegetation index data set for the period July 1981 to December 1999 can be summarized as follows:

1. About 61% of the total vegetated areas between 40°N and 70°N in Eurasia shows a persistent increase in growing season NDVI over a broad contiguous swath of land from central Europe through Siberia to the Aldan plateau, where 78% (9.8×10^6 km^2) is unmanaged, and almost 58% (7.3×10^6 km^2) is forests and woodlands, an area equivalent to about 78% of the United States. North America, in comparison,

shows a fragmented pattern of change in smaller areas notable only in the forests of the southeast and the grasslands of the upper Midwest.

2. Larger changes in both the magnitude and duration of the seasonal cycle of NDVI are observed in Eurasia compared with North America. NDVI in Eurasia (North America) increased by 12.41% (8.44%) during the growing season, from 1982 to 1999. A longer active growing season brought about by an early spring and delayed autumn is seen in Eurasia (18 ± 4 days), compared with North America (12 ± 5 days).

3. NDVI decreases are observed in parts of Alaska, boreal Canada, and northeastern Asia, possibly due to temperature-induced drought as these regions experienced pronounced warming without a concurrent increase in growing season precipitation [*Barber et al.*, 2000].

We argue that the changes in NDVI reflect changes in biological activity. Statistical analyses indicate that there is a statistically meaningful relation between changes in NDVI and land surface temperature for vegetated areas between 40°N and 70°N. That is, the temporal changes and continental differences in NDVI are consistent with ground-based measurements of temperature, an important determinant of biological activity.

Together, these results suggest a photosynthetically vigorous Eurasia relative to North America during the past two decades. This conclusion is inconsistent with the idea of a large terrestrial carbon sink in North America [*Fan et al.*, 1998] and consistent with forest inventory analyses [*Houghton et al.*, 1999; *United Nations*, 2000]. A recent comparative analysis of boreal and temperate forest inventory data of the 1980s and 1990s indicates a significant increase in

the size of the growing stock in the wilderness of former USSR as a result of dramatic decline in annual fellings [*United Nations*, 2000]. Additional corroboration from in situ data is required in view of the importance of growing season changes for carbon sequestration by vegetation [*Randerson et al.*, 1999], and understanding of both natural and socioeconomic processes that affect NDVI time series is also needed.

Normalized difference vegetation index data are only surrogates of plant photosynthetic activity, and the translation to actual photosynthetic gains requires additional research. Therefore the inferred changes in NDVI magnitude and growing season duration, together with the spatial persistence and trend patterns shown, must be interpreted cautiously; they suggest a photosynthetically vigorous Eurasia in comparison to North America between 1982 and 1998, possibly driven by temperature and precipitation patterns in the north. The majority of pixels with high persistence in NDVI increase in Eurasia, relative to North America, have higher NDVI averages and longer growing season durations than those with low persistence in NDVI increase. This suggests that maybe more than one mechanism is involved. The remarkable difference in growing season duration between Eurasia and North America may be a key reason.

The surface warming recorded by meteorological station thermometers globally during the past 25 years is especially pronounced on land in the north [*Hansen et al.*, 1999]. Whether this is related to unmitigated buildup of heat-trapping gases in the atmosphere is currently under study [*Barnett et al.*, 1999]; it does seem, however, that the birds [*Thomas and Lennon*, 1999], butterflies [*Parmesan et al.*, 1999], and boreal vegetation [*Keeling et al.*, 1996] have responded to the warm pulse.

References

Asner, G.P., A.R. Townsend, and B.H. Braswell, Satellite observation of El Niño effects on Amazon forest phenology and productivity, *Geophys. Res. Lett., 27*, 981-984, 2000.

Barber, V.A., G.P. Juday, and B.P. Finney, Reduced growth of Alaska white spruce in the twentieth century from temperature-induced drought stress, *Nature, 405*, 668-672, 2000.

Barnett, T.P., et al., Detection and attribution of recent climate change: A status report, *Bull. Am. Meteorol. Soc., 80*, 2631-2659, 1999.

Bradley, N.L., A.C. Leopold, J. Ross, and W. Huffaker, Phenological changes reflect climate change in Wisconsin, *Proc. Natl. Acad. Sci. U.S.A., 96*, 9701-9704, 1999.

Braswell, B.H., D.S. Schimel, E. Linder, and B. Moore, The response of global terrestrial ecosystems to interannual temperature variability, *Science, 278*, 870-872, 1997.

Brown, J.L., S. Li, and N. Bhagabati, Long-term trend toward earlier breeding in an American bird: A response to global warming?, *Proc. Natl. Acad. Sci. U.S.A., 96*, 5565-5569, 1999.

Colombo, S.J., Climatic warming and its effect on bud burst and risk of frost damage to white spruce in Canada, *For. Chron., 74*, 567-577, 1998.

Crick, H.Q.P., and T.H. Sparks, Climate change related to egg-laying trends, *Nature, 399*, 423-424, 1999.

DeFries, R., M. Hansen, J. Townshend, and R. Sohlberg, Global land cover classification at 8km spatial resolution: The use of training data derived from Landsat imagery in decision tree classifiers, *Int. J. Remote Sens., 19*, 3141-3168, 1998.

Dettinger, M.D., M. Ghil, C.M. Strong, W. Weibel, and P. Yiou, Software expedites singular-spectrum analysis of noisy time series, *Eos Trans. AGU, 76*, 12,14,21, 1995.

Dickey, D.A., and W.A. Fuller, Distribution of the estimators for autoregressive time series with a unit root, *J. Am. Stat. Assoc., 74*, 427-431, 1979.

Ebdon, D., Spatial relationships, in *Statistics in Geography*, pp. 150-163, Blackwell, Oxford, Great Britain, 1985.

Enders, W., Modeling economic time series: Trends and volatility, in *Applied Econometric Time Series*, edited by V. Barnett et al., pp. 135-210, John Wiley, New York, 1995.

Fan, S.M., M. Gloor, J. Mahlman, S. Pacala, J. Sarmiento, T. Takahashi, and P. Tans, A large terrestrial carbon sink in North America implied by atmospheric and oceanic carbon dioxide data and models, *Science, 282*, 442-446, 1998.

Folland, C.K., T. Karl, and K.Y. Vinnikov, Observed climate variability and change, in *Climate Change 1992: The Supplementary Report to the IPCC Scientific Assessment*, edited by J.T. Houghton, B.A. Callander, and S.K. Varney, pp.163, Cambridge Univ. Press, New York, 1992.

Fung, I.Y., C.J. Tucker, and K.C. Prentice, Application of very high resolution radiometer vegetation index to study atmosphere-biosphere exchange of CO_2, *J. Geophys. Res., 92*, 2999-3015, 1987.

Grace, J., and M. Rayment, Respiration in the balance, *Nature, 404*, 819-820, 2000.

Granger, C.W.J., and P. Newbold, Spurious regressions in econometrics, *J. Econometrics, 2*, 111-120, 1974.

Groisman, P.Y., T.R. Karl, and R.W. Knight, Observed impact of snow cover on the heat balance and the rise of continent spring temperature, *Science, 263*, 198-200, 1994.

Gutman, G., On the use of long-term global data of land reflectances and vegetation indices derived from the advanced very high resolution radiometer, *J. Geophys. Res., 104*, 6241-6255, 1999.

Gutman, G., and A. Ignatov, Global land monitoring from AVHRR: Potential and limitations, *Int. J. Remote Sens., 16*, 2301-2309, 1995.

Hansen, J., R. Ruedy, M. Sato, and R. Reynolds, Global surface air temperature in 1995: Return to pre-Pinatubo level, *Geophys. Res. Lett., 23*, 1665-1668, 1996.

Hansen, J., R. Ruedy, J. Glascoe, and M. Sato, GISS analysis of surface temperature change, *J. Geophys. Res., 104*, 30,997-31,022, 1999.

Holben, B.N., Characteristics of maximum value compositing imagines for AVHRR data, *Int. J. Remote Sens., 7*, 1417-1437, 1986.

Houghton, R.A., E.A. Davidson, and G.M. Woodwell, Missing sinks, feedbacks, and understanding the role of terrestrial ecosystems in the global carbon balance, *Global Biogeochem. Cycles, 12*, 25-34, 1998.

Houghton, R.A., J. L. Hackler, and K.T. Lawrence, The U.S. carbon budget: Contributions from land-use change, *Science, 285*, 574-578, 1999.

Huemmrich, K.F., T.A. Black, P.G. Jarvis, J.H. McCaughey, and F.G. Hall, High temporal resolution NDVI phenology from micrometeorological radiation sensors, *J. Geophys. Res., 104*, 27,935-27,944, 1999.

Jacquemoud, S., F. Baret, and J. F. Hanocq, Modeling spectral and bidirectional soil reflectance, *Remote Sens. Environ, 41*, 123-132, 1992.

Kaufmann, R.K., L. Zhou, Y. Knyazikhin, N. Shabanov, R. Myneni, and C. Tucker, Effect of orbital drift and sensor changes on the time series of AVHRR vegetation index data, *IEEE Trans. Geosci. Remote Sens., 38*, 2584-2597, 2000.

Keeling, C.D., J.F.S. Chin, and T.P. Whorf, Increased activity of northern vegetation inferred from atmospheric CO_2 measurements, *Nature, 382*, 146-149, 1996.

Konstantin, Y.V., A. Robock, R.J. Stouffer, J.E. Walsh, D.A. Robinson, D. Garrett, and V. Zakharov, Detection of global warming using observed Northern Hemisphere snow cover and sea ice areas, paper presented at The Tenth Symposium on Global Change Studies, Am. Meteorol. Soc., Dallas, Tex., 1999.

Los, S.O., Calibration adjustment of the NOAA-AVHRR normalized difference vegetation index without recourse to component channels 1 and 2 data, *Int. J. Remote Sens., 14*, 1907-1917, 1993.

Los, S.O., Estimation of the ratio of sensor degradation between

NOAA AVHRR channel 1 and 2 from monthly NDVI composites, *IEEE Trans. Geosci. Remote Sens., 36,* 202-213, 1998.

Los, S.O., C.O. Justice, and C.J. Tucker, A global 1° x 1° NDVI data set for climate studies derived from the GIMMS continental NDVI data, *Int. J. Remote Sens., 15,* 3493-3518, 1994.

Mann, M.E., R.S. Bradley, and M.K. Hughes, Global-scale temperature patterns and climate forcing over the past six centuries, *Nature, 392,* 779-787, 1998.

Menzel, A., and P. Fabian, Growing season extended in Europe, *Nature, 397,* 659-659, 1999.

Myneni, R.B., F. G. Hall, P.J. Sellers, and A.L., Marshak, The interpretation of spectral vegetation indexes, *IEEE Trans. Geosci. Remote Sens., 33,* 481-486, 1995.

Myneni, R.B., S.O. Los, and C.J. Tucker, Satellite-based identification of linked vegetation index and sea surface temperature anomaly areas from 1982-1990 for Africa, Australia and South America, *Geophys. Res. Lett., 23,* 729-732, 1996.

Myneni, R.B., C.D. Keeling, C.J. Tucker, G. Asrar, and R.R. Nemani, Increased plant growth in the northern high latitudes from 1981-1991, *Nature, 386,* 698-702, 1997.

Myneni, R.B., C.J. Tucker, G. Asrar, and C.D. Keeling, Interannual variations in satellite-sensed vegetation index data from 1981 to 1991, *J. Geophys. Res., 103,* 6145-6160, 1998.

Nelson, C. R., and C. I. Plosser, Trends and random walks in macroeconomic time series: some evidence and implications, *J. Monetary Econ., 10,* 139-162, 1982.

Parmesan, C., et al., Poleward shifts in geographical ranges of butterfly species associated with regional warming, *Nature, 399,* 579-583, 1999.

Privette, J.L., C. Fowler, G.A. Wick, D. Baldwin, and W.J. Emery, Effect of orbital drift on advanced very high resolution radiometer products: Normalized difference vegetation index and sea surface temperature, *Remote Sens. Environ., 53,* 164-171, 1995.

Randerson, J.T., C.B. Field, I.Y. Fung, and P.P. Tans, Increases in early season ecosystem uptake explain recent changes in the seasonal cycle of atmospheric CO_2 at high northern latitudes, *Geophys. Res. Lett., 26,* 2765-2769, 1999.

Rao, C.R.N., and J. Chen, Inter-satellite calibration linkages for the visible and near-infrared channels of the advanced very high resolution radiometer on the NOAA-7, -9, -11 spacecraft, *Int. J. Remote Sens., 16,* 1931-1942, 1995.

Rao, C.R.N., and J. Chen, Post-launch calibration of the visible and near-infrared channels of the advanced very high resolution radiometer on the NOAA-14 spacecraft, *Int. J. Remote Sens., 17,* 2743-2747, 1996.

Rosborough, G.W., D.G. Baldwin, and W.J. Emery, Precise AVHRR image navigation, *IEEE Trans Geosci. Remote Sens., 32,* 644-657, 1994.

Sato, M., J.E. Hansen, M.P. McCormick, and J.B. Pollack, Stratospheric aerosol optical depth, 1850-1990, *J. Geophys. Res., 98,* 22,987-22,994, 1993.

Schimel, D.S., D. Alves, I. Enting, M. Heimann, F. Joos, D.

Raynaud, and T. Wigley, CO_2 and the carbon cycle, in *Climate Change 1995: The Science of Climate Change,* edited by J.T. Houghton et al., pp. 76-86, Cambridge Univ. Press, New York, 1996.

Schwartz, M.D, Green-wave phenology, *Nature, 394,* 839-840, 1998.

Tans, P.P., I.Y. Fung, and T. Takahashi, Observation constraints on the global atmospheric CO_2 budget, *Science, 247,* 1431-1438, 1990.

Thomas, C.D., and J.J. Lennon, Birds extend their ranges northwards, *Nature, 399,* 213-213, 1999.

Tucker, C.J., W.W. Newcomb, and H.E Dregne, AVHRR data sets for determination of desert spatial extent, *Int. J. Remote Sens., 15,* 3547-3565, 1994.

United Nations, Woody biomass and the carbon cycle, in *Chapter IIIb: Forest Resources of Europe, GIS, North America, Australia, Japan and New Zealand (Industrialized temperate/boreal countries), UN-ECE/FAO contribution to the Global Forest Resource Assessment 2000,* pp. 27-41, New York, 2000.

Vaganov, E.A., M.K. Hughes, A.V. Kirdyanov, F.H. Schweingruber, and P.P. Silkin, Influence of snowfall and melt timing on tree growth in subarctic Eurasia, *Nature, 400,* 149-151, 1999.

Valentini, R., et al., Respiration as the main determinant of carbon balance in European forests, *Nature, 404,* 861-864, 2000.

Vatuard, R., P. Yiou, and M. Ghil, Singular-spectrum analysis: A toolkit for short, noisy chaotic signals, *Physica D, 58,* 95-126, 1989.

Vermote, E.E., and N.Z. El Saleous, Stratospheric aerosol perturbing effect on remote sensing of vegetation: Operational method for the correction of AVHRR composite NDVI, *SPIE Atmos. Sens. Model., 2311,* 19-29, 1994.

Vermote, E.F., and Y.J. Kaufman, Absolute calibration of AVHRR visible and near-infrared channels using ocean and cloud views, *Int. J. Remote Sens., 16,* 2317-2340, 1995.

Zimov, S.A, S.P. Davidov, G.M. Zimova, A.I. Davidova, F.S. Chapin III, M.C. Chapin, and J.F. Reynolds, Contribution of disturbance to increasing seasonal amplitude of atmospheric CO_2, *Science, 284,* 1973-1976, 1999.

R.K. Kaufmann, R.B. Myneni, N.V. Shabanov, and L. Zhou, Department of Geography, 675 Commonwealth Avenue, Boston University, Boston, MA 02215, USA. (email: kaufmann@bu.edu; rmyneni@crsa.bu.edu; shabanov@bu.edu; lmzhou@crsa.bu.edu.)

D. Slayback, Science Systems and Applications Inc., Biospheric Sciences Branch, Code 923, NASA Goddard Space Flight Center, Greenbelt, MD 20771, USA. (email: dan@manyu.gsfc.nasa.gov)

C.J. Tucker, Biospheric Sciences Branch, Code 923, NASA Goddard Space Flight Center, Greenbelt, MD 20771, USA. (email: compton@kratmos.gsfc.nasa.gov)